NASA Micropulse Lidar Rain Algorithm

Precipitation modifies atmospheric column thermodynamics through the process of evaporation and serves as a proxy for latent heat modulation. For this reason, a correct precipitation parameterization (especially for low-intensity precipitation) within global scale models is crucial. In addition to improving our modeling of the hydrological cycle, this will reduce the associated uncertainty of global climate models in correctly forecasting future scenarios, and will enable the application of mitigation strategies. In this study we present a proof of concept algorithm to automatically detect precipitation from lidar measurements obtained from the National Aeronautics and Space Administration Micropulse lidar network (MPLNET).

1. Introduction

Human life is strongly dependent on the water cycle [1]. In particular, precipitation is a key-player in pairing the Earth–atmosphere water and energy cycle, through modulating atmospheric column latent heat and affecting cloudiness and cloud lifetime. For this reason, long-term precipitation datasets are needed to analyze spatial and temporal trends and variability, especially at the global scale [2]. In the last two decades, thanks to the internet, a ground-based network of instruments has started to develop and measure important climate-related variables [3], including columnar and atmospheric profiles of aerosol optical and micro-physical properties through passive and active optical sensors (i.e., sunphotometers and lidars). Nevertheless, elastic [4] multi-wavelength and Doppler lidar observations containing raining events are usually unjustifiably disregarded in standard monitor activities, even if light rain events are clearly detectable on lidar data [5].

Some recent studies show that a correct precipitation parameterization [6] will drastically improve global climate models to forecast future scenarios that can help define the best mitigation and adaptation strategies. Further, precipitation studies are crucial to assessing aerosol indirect and semi-direct effects, since aerosols influence both cloud formation and precipitation that in turn removes aerosols from the atmosphere by scavenging effect. Isolated case studies using lidar data (together with ancillary instrumentation) to quantitatively assess the atmospheric profile of precipitation micro-physical and optical characteristics are shown in [5][7][8][9][10]. Nevertheless, these efforts, due to their intrinsic complexity, are not suitable to be operationally implemented in a network of instruments.

Several studies showing the development of aerosol [11][12] and cloud [13] masking algorithms exist, but, to our knowledge, none demonstrate automatically detecting light rain events using lidar observations. In this paper we present a proof-of-concept rain masking algorithm and report results of an intercomparison with a disdrometer to prove the efficacy of the algorithm in detecting light rain, drizzle, and virga events from lidar observations. The algorithm, once extensively tested and validated also against other remote sensing instruments (i.e., high-frequency radars) will be implemented in the National Administration and Space Agency (NASA) Micropulse lidar network (MPLNET https://mplnet.gsfc.nasa.gov/; see Section 3) and will provide, when available, a new complimentary rain mask variable that can be used either as the starting point to further investigating scientifically interesting-precipitation cases (i.e., to assess their optical and micro-physical properties, [5][7][8][9]) or simply to better characterize precipitation patterns and its variability at different spatial scales.

The developed algorithm, based on image processing techniques, applies morphological filters on composite plots of the Volume Depolarization Ratio (VDR) variable, as defined in [14] and this algorithm will permit MPLNET to fill the gap left by the joint NASA and Japan Aerospace Exploration Agency (JAXA) missions, as the Tropical Rainfall Measuring Mission (TRMM) followed by the Global Precipitation Measurement (GPM) [15], in detecting low intensity precipitation [5], especially at mid and higher latitudes [16]. Our paper is outlined as follows: in Section 3 we describe in detail the NASA MPLNET network and its products used as input by the rain masking algorithm. Section 4 shows the algorithm flowchart and all the

different phases from input to output are carefully described. Section 5 reports the algorithm intercomparison and validation through co-located ground-based observations by disdrometer, while in Section 6 discussion and future perspectives are reported.

2. The MicroPulse Lidar Network

The NASA MPLNET network [17], active since 1999, is a federated network of commercially–available Micropulse lidar (MPL) systems [18], produced by LEICA Geosystems, Lanham, MD, USA (formerly SigmaSpace). The instruments, active optical devices that have developed since CO_2 laser invention [19], are globally deployed to support the NASA Earth Observing System (EOS) program [20]. The MPLNET lidar network continuously monitors the atmosphere every 60 s, from the surface up to 30 km with a software-adjustable vertically-resolved spatial resolution (depending on the station, 0.030–0.075 km), under any meteorological condition and to the limit of laser signal attenuation. Both temporary and permanent observational sites are globally deployed, and are located at polar, mid-latitudes, tropical, and equatorial regions to retrieve the aerosol [21][22][23], cloud optical [24][25], and geometrical properties together with their radiative effects. The single-wavelength MPL lidar system, is co-located, when possible, together with the NASA Aerosol Robotic Network (AERONET; [26]) sunphotometer to reduce error in retrievals [27]. MPLNET products are freely and publicly available at the MPLNET website, which follows the modified EOS convention as: Level 1, Level 1.5, and Level 2, are all available in near real time (NRT). The only difference between L1 and L15 products are that data failing to meet the L15 Quality Assurance (QA) criteria are screened and replaced with Not a Number (NaN) in the files. The primary difference between L2 and L1/15 files is that L2 may have additional post-calibrations applied as well as corrections to instrument temperatures.

Since 2017, MPLNET has fully integrated polarized MPL systems into the network, which provides information about particle shape. Each instrument relies on the collection of two-channel measurements (i.e., the signal measure $P_{co}(z)$ and $P_{cr}(z)$). A detailed description of the depolarization channel can be found in [14]. Even a half degree tilting of the lidar instrument with respect to the vertical direction, needed to avoid cirrus cloud specular reflection, is sufficient to substantially increase the VDR of the precipitation (even for spherical raindrops), as shown in [28]. This rain enhanced contrast in lidar VDR composite images facilitates its detection. Figure 1 shows a front descent on 27 March 2018 with multiple rainfall episodes showing higher VDR values (green bins). The start of the precipitation event is highlighted by red arrows.
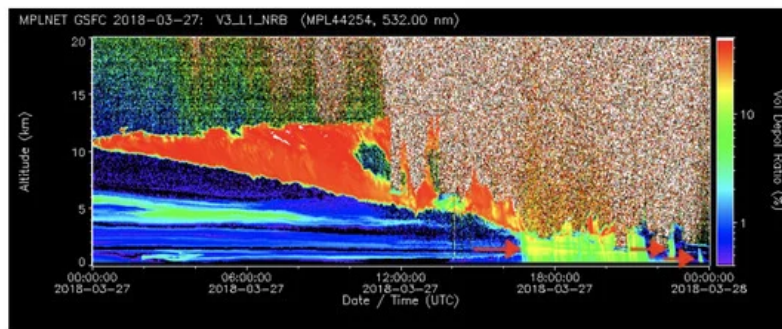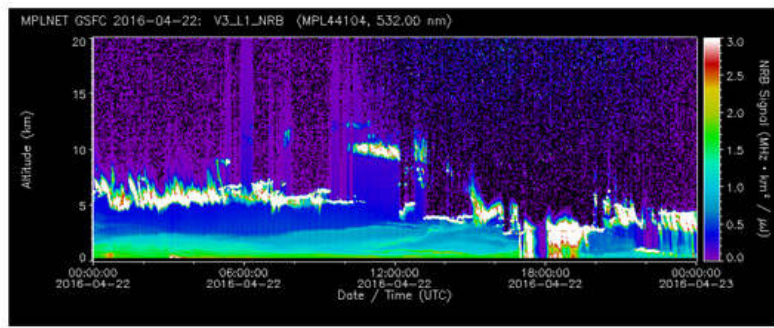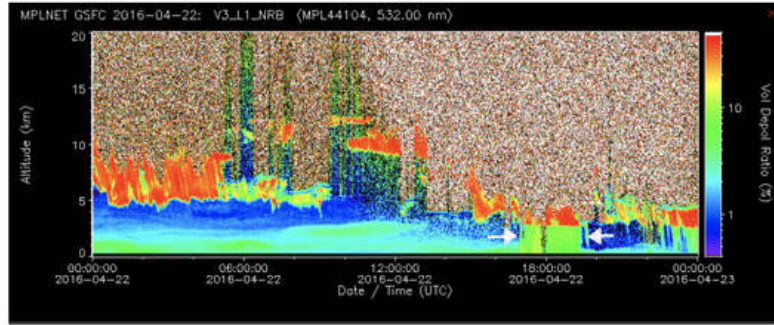

Figure 1. 27 March 2017 Micropulse lidar network (MPLNET) Version 3 Volume Depolarization Ratio (VDR) variable (L15 MPLNET Normalized Relative Backscattering (NRB) product). Red arrows highlight the starting point of the precipitation events.

The proposed algorithm, uses, as the input composite image, the new Version 3 (V3) VDR variable, paired with the cloud mask [13] variable found in the L15 Normalized Relative Backscatter (NRB) and Cloud (CLD) data products [27][29], respectively. The cloud mask is an array of integer numbers where cloudy bins are labeled as 2, non-cloudy bins as 1, while bins with an indistinguishable signal-to-noise ratio are labeled as 4. For image-based detection techniques, the L15 NRB VDR variable is preferred to the L15 NRB variable (i.e., the backscattered energy by the atmosphere) as in the VDR variable composite images the rainfall bins show a higher volume depolarization ratio. This translates into higher contrast, as shown in Figure 2b.

(a) NRB variable composite image on 22 April 2016 observed at National Administration and Space Agency (NASA) Goddard Space Flight Center permanent MPLNET observational site.

(b) VDR variable composite image on 22 April 2016 observed at NASA Goddard Space Flight Center permanent MPLNET observational site. The rainfall event has a different color with respect to the background aerosol (greener tone), while clouds are represented in red.

Figure 2. Precipitation event detected on 22 April 2016. With respect to (**a**) NRB, the precipitation on (**b**) VDR has more defined and sharp contours. The precipitation under the cloud (in red) has a different green tone. For this reason, the detection is easier on (**b**).

It is clearly visible that, with respect to the strong red depolarizing structures (VDR>35%) (e.g., clouds containing ice), the signal assumes a well-defined rectangular shape that can be identified as rainfall. In contrast, during non-rain episodes, the signal does not assume a particular shape and the VDR shows lower values.

3. Discussion and Conclusions

Automated networks of instruments started to develop in the last two decades aiming to continuously monitor crucial atmospheric physical, thermodynamic, geometrical, and optical variables. Among them, the NASA MicroPulse Lidar NETwork (MPLNET), active since 1999, has globally deployed more than 21 worldwide observational sites in the tropics, mid-latitudes, and polar regions in both hemispheres to automatically retrieve 24/24 the geometrical and optical properties of aerosol and cloud atmospheric profiles under any meteorological conditions. Despite that lidar has proven to be very effective in detecting especially light precipitation and drizzle, lidar data containing precipitation episodes are currently unjustifiably disregarded. As a proof of concept, in this study we developed a rain masking algorithm, based on the volume depolarization ratio variable, which is proven to be effective in detecting light rain, drizzle, and virga episodes. Once rigorously validated and operationally implemented into the NASA MPLNET lidar network, the rain masking algorithm will consistently help in understanding how light precipitation contributes to cloud formation and will fill a gap left by TRMM and GPM missions in detecting low intensity rainfall episodes. This is crucial to improving global climate model forecasts and for aerosol–clouds and in turn, precipitation interactions. Finally, as future development, the algorithm will be also tested on simpler elastic lidar instruments without the depolarization channel, i.e., the ceilometers, to assess the rain detection feasibility. In more detail, precipitation is a fundamental meteorological phenomenon that is the principal responsible for atmospheric aerosol removal. Analyzing a large database of lidar measurements will help in fully characterizing the aerosol cycle, from emission to deposition, and validate global model observations that show a strong negative correlation between Aerosol Optical Depth (AOD) and precipitation due to wet scavenging [30]. A synergy between both passive and active satellite NASA missions, i.e., the Moderate Resolution Imager Spectrometer (MODIS; [31] and the Cloud-Aerosol Lidar and Infrared Pathfinder Satellite Observation (CALIPSO; [32]), and the ground based lidar networks, such as the European Aerosol LIdar NETwork (EARLINET; [33]) part of the Aerosols, Clouds and Trace gases Research Infrastructure (ACTRIS http://www.actris.eu) and in North America as MPLNET, and more in general in the frame of Global Aerosol Watch (GAW) aerosol lidar observation network (GALION; [34]) will strongly contribute to quantitatively assess how the above cloud aerosol load influences clouds and then rainfalls. The synergy will then assess the "all-sky" aerosol contribution to clouds and precipitation.

The image-based technique methodology used in developing the proposed algorithm, will be tested in a future work over different instruments, i.e., ceilometers, where precipitation still looks like a higher-contrasted feature in the range corrected backscattered energy.

References

1. Bosilovich, M.G.; Schubert, S.D.; Walker, G.K. Global Changes of the Water Cycle Intensity. J. Clim. 2005, 18, 1591–1608.

2. Koster, R.D.; Suarez, M.J.; Heiser, M. Variance and Predictability of Precipitation at Seasonal-to-Interannual Timescales. J. Hydrometeorol. 2000, 1, 26–46.

3. Lolli, S.; Di Girolamo, P. Principal component analysis approach to evaluate instrument performances in developing a cost-effective reliable instrument network for atmospheric measurements. J. Atmos. Ocean. Technol. 2015, 32, 1642–1649.

4. Lolli, S.; Delaval, A.; Loth, C.; Garnier, A.; Flamant, P. 0.355-micrometer direct detection wind lidar under testing during a field campaign in consideration of ESA's ADM-Aeolus mission. Atmos. Meas. Tech. 2013, 6, 3349–3358.

5. Lolli, S.; D'Adderio, L.; Campbell, J.; Sicard, M.; Welton, E.; Binci, A.; Rea, A.; Tokay, A.; Comerón, A.; Baldasano, J.M.; et al. Vertically Resolved Precipitation Intensity Retrieved through a Synergy between the Ground-Based NASA MPLNET Lidar Network Measurements, Surface Disdrometer Datasets and an Analytical Model Solution. Remote Sens. 2018, 10, 1102.

6. Campbell, J.R.; Ge, C.; Wang, J.; Welton, E.J.; Bucholtz, A.; Hyer, E.J.; Reid, E.A.; Chew, B.N.; Liew, S.C.; Salinas, S.V.; et al. Applying advanced ground-based remote sensing in the Southeast Asian Maritime Continent to characterize regional proficiencies in smoke transport modeling. J. Appl. Meteorol. Climatol. 2016, 55, 3–22.

7. Westbrook, C.; Hogan, R.; O'Connor, E.; Illingworth, A. Estimating drizzle drop size and precipitation rate using two-colour lidar measurements. Atmos. Meas. Tech. 2010, 3, 671–681.

8. Lolli, S.; Welton, E.J.; Campbell, J.R. Evaluating light rain drop size estimates from multiwavelength micropulse lidar network profiling. J. Atmos. Ocean. Technol. 2013, 30, 2798–2807.

9. Lolli, S.; Di Girolamo, P.; Demoz, B.; Li, X.; Welton, E. Rain Evaporation Rate Estimates from Dual-Wavelength Lidar Measurements and Intercomparison against a Model Analytical Solution. J. Atmos. Ocean. Technol. 2017, 34, 829–839.

10. D'Adderio, L.; Porcù, F.; Tokay, A. Evolution of drop size distribution in natural rain. Atmos. Res. 2018, 200, 70–76.

11. Omar, A.H.; Winker, D.M.; Vaughan, M.A.; Hu, Y.; Trepte, C.R.; Ferrare, R.A.; Lee, K.P.; Hostetler, C.A.; Kittaka, C.; Rogers, R.R.; et al. The CALIPSO automated aerosol classification and lidar ratio selection algorithm. J. Atmos. Ocean. Technol. 2009, 26, 1994–2014.

12. Papagiannopoulos, N.; Mona, L.; Amodeo, A.; D'Amico, G.; Gumà Claramunt, P.; Pappalardo, G.; Alados-Arboledas, L.; Guerrero-Rascado, J.L.; Amiridis, V.; Kokkalis, P.; et al. An automatic observation-based aerosol typing method for EARLINET. Atmos. Chem. Phys. 2018, 18, 15879–15901.

13. Lewis, J.R.; Campbell, J.R.; Welton, E.J.; Stewart, S.A.; Haftings, P.C. Overview of MPLNET Version 3 Cloud Detection. J. Atmos. Ocean. Technol. 2016, 33, 2113–2134.

14. Flynn, C.J.; Mendoza, A.; Zheng, Y.; Mathur, S. Novel polarization-sensitive micropulse lidar measurement technique. Opt. Express 2007, 15, 2785–2790.

15. Hou, A.Y.; Kakar, R.K.; Neeck, S.; Azarbarzin, A.A.; Kummerow, C.D.; Kojima, M.; Oki, R.; Nakamura, K.; Iguchi, T. The Global Precipitation Measurement Mission. Bull. Am. Meteorol. Soc. 2014, 95, 701–722.

16. Kidd, C.; Joe, P. Importance, identification and measurement of light precipitation at mid-to high-latitudes. In Proceedings of the Joint EUMETSAT Meteorological Satellite Conference and 15th Satellite Meteorology and Oceanography Conference, Amsterdam, The Netherlands, 24–28 September 2007; pp. 24–28.

17. Welton, E.J.; Campbell, J.R.; Spinhirne, J.D.; Stanley Scott, V., III. Global monitoring of clouds and aerosols using a network of micropulse lidar systems. SPIE Conf. Proc. 2001, 4153, 151–158.

18. Spinhirne, J.D.; Rall, J.A.; Scott, V.S. Compact Eye Safe Lidar Systems. Rev. Laser Eng. 1995, 23, 112–118.

19. Ciofini, M.; Lapucci, A.; Lolli, S. Diffractive optical components for high power laser beam sampling. J. Opt. Pure Appl. Opt. 2003, 5, 186.

20. Wielicki, B.A.; Cess, R.D.; King, M.D.; Randall, D.A.; Harrison, E.F. Mission to planet Earth: Role of clouds and radiation in climate. Bull. Am. Meteorol. Soc. 1995, 76, 2125–2154.

21. Pani, S.K.; Wang, S.H.; Lin, N.H.; Tsay, S.C.; Lolli, S.; Chuang, M.T.; Lee, C.T.; Chantara, S.; Yu, J.Y. Assessment of aerosol optical property and radiative effect for the layer decoupling cases over the northern South China Sea during the 7-SEAS/Dongsha Experiment. J. Geophys. Res. Atmos. 2016, 121, 4894–4906.

22. Tosca, M.G.; Campbell, J.; Garay, M.; Lolli, S.; Seidel, F.C.; Marquis, J.; Kalashnikova, O. Attributing accelerated summertime warming in the southeast united states to recent reductions in aerosol burden: Indications from vertically-resolved observations. Remote Sens. 2017, 9, 674.

23. Lolli, S.; Madonna, F.; Rosoldi, M.; Campbell, J.R.; Welton, E.J.; Lewis, J.R.; Gu, Y.; Pappalardo, G. Impact of varying lidar measurement and data processing techniques in evaluating cirrus cloud and aerosol direct radiative effects. Atmos. Meas. Tech. 2018, 11, 1639.

24. Campbell, J.R.; Lolli, S.; Lewis, J.R.; Gu, Y.; Welton, E.J. Daytime cirrus cloud top-of-the-atmosphere radiative forcing properties at a midlatitude site and their global consequences. J. Appl. Meteorol. Climatol. 2016, 55, 1667–1679.

25. Lolli, S.; Campbell, J.R.; Lewis, J.R.; Gu, Y.; Marquis, J.W.; Chew, B.N.; Liew, S.C.; Salinas, S.V.; Welton, E.J. Daytime Top-of-the-Atmosphere Cirrus Cloud Radiative Forcing Properties at Singapore. J. Appl. Meteorol. Climatol. 2017, 56, 1249–1257.

26. Holben, B.; Eck, T.; Slutsker, I.; Tanré, D.; Buis, J.; Setzer, A.; Vermote, E.; Reagan, J.; Kaufman, Y.; Nakajima, T.; et al. AERONET—A Federated Instrument Network and Data Archive for Aerosol Characterization. Remote Sens. Environ. 1998, 66, 1–16.

27. Welton, E.J.; Campbell, J.R. Micropulse Lidar Signals: Uncertainty Analysis. J. Atmos. Ocean. Technol. 2002, 19, 2089–2094.

28. Bissonnette, L.R.; Roy, G.; Fabry, F. Range–Height Scans of Lidar Depolarization for Characterizing Properties and Phase of Clouds and Precipitation. J. Atmos. Ocean. Technol. 2001, 18, 1429–1446.

29. Campbell, J.R.; Hlavka, D.L.; Welton, E.J.; Flynn, C.J.; Turner, D.D.; Spinhirne, J.D.; Scott, V.S.; Hwang, I.H. Full-Time, Eye-Safe Cloud and Aerosol Lidar Observation at Atmospheric Radiation Measurement Program Sites: Instruments and Data Processing. J. Atmos. Ocean. Technol. 2002, 19, 431–442.

30. Gryspeerdt, E.; Stier, P.; White, B.A.; Kipling, Z. Wet scavenging limits the detection of aerosol effects on precipitation. Atmos. Chem. Phys. 2015, 15, 7557–7570.

31. Remer, L.A.; Kaufman, Y.; Tanré, D.; Mattoo, S.; Chu, D.; Martins, J.V.; Li, R.R.; Ichoku, C.; Levy, R.; Kleidman, R.; et al. The MODIS aerosol algorithm, products, and validation. J. Atmos. Sci. 2005, 62, 947–973.

32. Hunt, W.H.; Winker, D.M.; Vaughan, M.A.; Powell, K.A.; Lucker, P.L.; Weimer, C. CALIPSO lidar description and performance assessment. J. Atmos. Ocean. Technol. 2009, 26, 1214–1228.

33. Pappalardo, G.; Amodeo, A.; Apituley, A.; Comeron, A.; Freudenthaler, V.; Linné, H.; Ansmann, A.; Bösenberg, J.; D'Amico, G.; Mattis, I.; et al. EARLINET. Atmos. Meas. Tech. 2014, 7, 2389–2409.

34. Bösenberg, J.; Hoff, R. Plan for the Implementation of the GAW Aerosol Lidar Observation Network GALION:(Hamburg, Germany, 27–29 March 2007); GAW Report 178; WMO: Geneva, Switzerland, 2007.